



## OpenAIR@RGU

### The Open Access Institutional Repository at Robert Gordon University

<http://openair.rgu.ac.uk>

This is an author produced version of a paper published in

Journal of Luminescence (ISSN 0022-2313)

This version may not include final proof corrections and does not include published layout or pagination.

#### Citation Details

##### Citation for the version of the work held in 'OpenAIR@RGU':

**PETER, J., KUMAR, M., ANANAD, V. R., SALEEM, R., SEBASTIAN, A., RADHAKRISHNAN, P., NAMPOORI, V. P. N., VALLABHAN, C. P. G., PRABHU, R., and KAILASNATH, M., 2016. Solvent effects on lasing characteristics for Rh B laser dye. Available from *OpenAIR@RGU*. [online]. Available from: <http://openair.rgu.ac.uk>**

##### Citation for the publisher's version:

**PETER, J., KUMAR, M., ANANAD, V. R., SALEEM, R., SEBASTIAN, A., RADHAKRISHNAN, P., NAMPOORI, V. P. N., VALLABHAN, C. P. G., PRABHU, R., and KAILASNATH, M., 2016. Solvent effects on lasing characteristics for Rh B laser dye. *Journal of Luminescence*, Vol. 169 (A), pp. 227-232.**



**This work is licensed under a Creative Commons Attribution - Non-Commercial - No-Derivatives 4.0 International Licence**

#### Copyright

Items in 'OpenAIR@RGU', Robert Gordon University Open Access Institutional Repository, are protected by copyright and intellectual property law. If you believe that any material held in 'OpenAIR@RGU' infringes copyright, please contact [openair-help@rgu.ac.uk](mailto:openair-help@rgu.ac.uk) with details. The item will be removed from the repository while the claim is investigated.

© 2016. This manuscript version is made available under the CC-BY-NC-ND 4.0 license <http://creativecommons.org/licenses/by-nc-nd/4.0/>

<http://dx.doi.org/10.1016/j.jlumin.2015.09.002>

# Solvent effects on lasing characteristics for Rh B laser dye

Jaison Peter<sup>\*1</sup>, Mahesh Kumar<sup>2</sup>, V. R. Ananad<sup>1</sup>, Rasool Saleem<sup>1</sup>, Ananthu Sebastian<sup>1</sup>, P. Radhakrishnan<sup>1</sup>, V. P. N. Nampoori<sup>1</sup>, C. P. G. Vallabhan<sup>1</sup>, Radhakrishna Prabhu<sup>3</sup>, and M. Kailasnath<sup>1</sup>

<sup>1</sup>International School of Photonics, Cochin University of Science and Technology, Cochin 682022, India

<sup>2</sup>Department of Applied Chemistry, Cochin University of Science and Technology, Cochin 682022, India

<sup>3</sup>School of Engineering, Robert Gordon University, Aberdeen, AB10 1FR, Scotland, UK

\*Corresponding author: jaison.peter@gmail.com

**Abstract:** We demonstrate pulsed, photopumped multimode laser emission in the visible spectral range from rhodamine B dye dissolved in various solvents. The laser emission is characterized by a well-defined, low threshold pump power at which the emission spectral intensity dramatically increases and collapsed into several dominant laser modes with reduced mode spacing and spectral width. The modes were found to originate from the subcavities formed by the plane-parallel walls of the cuvette containing the gain medium. The cavity lasing spectral structure and the numbers of longitudinal modes were easily controlled by changing the solvents. A shift in the emission spectra has been also observed by changing the solvents will allow a limited range of tuning of laser emission wavelength. We also determined the gain coefficient and stimulated emission cross-section for the Rh B dye dissolved liquid laser system. A detailed discussion of the solvent effect in the lasing characteristics of Rh B in different solution is explained along with the computational data.

## 1. Introduction

The first laser was built in 1960 by Maiman [1], 44 years after Einstein's discovery of stimulated emission. Six years after, the first dye laser was realized by Sorokin and Lankard [2]. The ultra-wide wavelength tuning range and the ability to generate both narrow linewidth continuous wave output and ultra-short pulses make dye lasers an ideal coherent source for spectroscopy [3]. Generally, laser dyes are complex organic molecules containing long chains of conjugated double bonds. The complex molecular structure will lead to many vibrational and rotational energy levels within a single electronic state. Therefore, laser dyes often have strong and wide absorption bands in the UV and visible region [4-5]. Liquid dye lasers are the first material systems used to study the laser action and other optical processes in microcavities. In liquid dye lasers, tuning of the laser wavelength is performed either by changing the concentration of the dye, *concentration tuning* or by changing the optical path length in the cavity. To change the optical path of the cavity, the solvent of the dye can be changed, thereby changing the refractive index in the cavity. This method is so called *solvent tuning*. One should keep in mind that by changing the solvent, other properties of the fluid which can affect the laser wavelength may be changed due to the interaction between dye molecules and the solvent molecules.

The solvent plays an important role in photophysical properties of laser dye. In this paper, we analyze the solvent effects on the laser emission characteristics for Rhodamine B (Rh B) laser dye. In our study, Rh B dye is dissolved in different solvents such as ethanol, methanol, butanol, ethylene glycol and glycerol, which are pumped longitudinally with short light pulses of several energies [6-7]. Apart from its particularly large cross section, it has high photochemical stability, which is important in practice to withstand multiple excitation cycles with a pulsed pump laser. Organic laser dyes typically show a large fluorescence yield ranging from about 0.6 to near the optimum 1.0. Figure 1 shows the absorption spectra of Rh B with a concentration of  $5 \times 10^{-4}$  mol/dm<sup>3</sup>, which is dissolved in ethanol, butanol and glycerol respectively. These spectra were measured in a cuvette of diameter 0.1 cm using a UV-VIS spectrophotometer (Jasco V-570). The absorption spectra exhibit a solvatochromic shift after exchange between one solvent to another. Due to the electron redistribution within the solvent molecules, the energy difference between the ground state and excited states will vary.

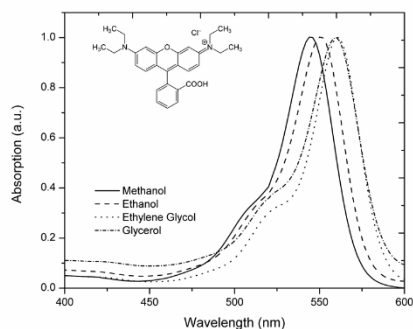


Fig. 1. Absorption spectra of Rh B dye ( $5 \times 10^{-4} \text{ mol/dm}^3$ ) dissolved in various solvent. Inset shows the molecular formula of Rh B.

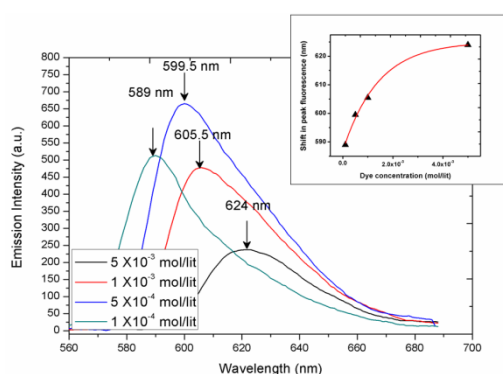


Fig. 2. Fluorescence spectra of Rh B dye dissolved in methanol with different concentration. Inset shows red-shift of peak fluorescence with the concentration of Rh B.

Figure 2 shows the tuning of emission wavelength peak with variation in the dye concentration in methanol. The peak emission wavelength of Rh B dye with  $1 \times 10^{-4} \text{ mol/dm}^3$  concentration is found to be at 589 nm. By increasing the concentration of Rh B, the peak wavelength shows a clear redshift and at  $5 \times 10^{-3} \text{ mol/dm}^3$  concentration the emission peak is at 624 nm. Due to Stokes shift, the shorter wavelength of emission spectrum is absorbed by Rh B molecule and re-emit to the higher wavelength. The increase in concentration will increase the interaction between the dye molecules and the fluorescence light will result the shifting of the emitted fluorescence peak towards the longer wavelength region. This type of concentration dependent red-shift was also reported by F. P. Schafer [3]. These types of tuning of the emission wavelength by changing the concentration of the dye are generally known as *concentration tuning*. The inset of figure 2 shows the redshift of emission spectra as a function of dye concentration. From this, it is clear that the lasing wavelength is tunable over a wide range (589-624 nm) due to the overlap of absorption and emission spectra of Rh B dye. However, after a particular dye concentration, the shift tends to exhibit saturation behavior.

## 2. Experimental setup

To observe lasing from the different dye solution, we used the second harmonic output of a Q-switched Nd:YAG laser that emits pulses of 8 ns duration at a repetition rate of 10 Hz as the excitation source. The pump power was adjusted with neutral density filters, and focused by a cylindrical lens into a  $0.2 \text{ mm} \times 4 \text{ mm}$  stripe transverse to a quartz cuvette of 1 cm inner length that contained dye solution. The schematic of the experimental setup is shown in the left inset of figure 3. This optical setup induces amplified spontaneous emission (ASE) along with the gain guiding and laser emission. The parallel windows of the quartz cuvette will provide the optical feedback, which is necessary for laser action. The emissions guided along the excitation stripe were collected from the side of the cuvette using a collecting fiber, and were then spectrally analyzed using a spectrometer and a charge coupled device. All the investigations were done in Rh B dye solutions with a constant dye concentration of  $5 \times 10^{-4} \text{ mol/dm}^3$  in different solvents, while all the experimental conditions such as pump power, ambient temperature, excitation length of the gain medium and mode of collection remained the same.

## 3. Photophysical properties of dye

The unique features of dye lasers are directly linked to the molecular structure and the photophysical properties of organic dye molecules. The complex molecular structure also leads to many vibrational and rotational levels within the single electronic state. The effective homogeneous line-broadening mechanism due to the collision with solvent molecules smears these sublevels into unresolved overlapping bands. The homogeneous broadened

spectra of dye molecules enable very efficient channeling of pump power into narrow band laser emission. Dye laser can be considered as a classical four level system (for simplicity, just neglect the triplet state). Under optical excitation, dye molecules are pumped from ground state  $S_0$  ( $v = 0$ ) to some vibrational-rotational sublevels in the first excited singlet state  $S_1$  ( $v \neq 0$ ) as marked as I in figure 3 (This vertical line represent the absorption line of dye molecule). The dye molecules in this level will quickly relax to the bottom of  $S_1$  ( $v = 0$ ) (the lowest rotational-vibrational sublevel). This non-radiative decay process happens on the time scale of a few pico-seconds or less (This is represented by II). This energy lost in the process contribute to the heating of solvents. From the upper laser level, dye molecules can undergo either spontaneous emission or stimulated emission into some rotational-vibrational sublevel in  $S_0$  ( $v \neq 0$ ) marked as III. This vertical line represent the emission line of dye molecules. Due to fast non-radiative decay, the molecules are quickly relax into the bottom of the ground state  $S_0$  ( $v = 0$ ) within a few pico-seconds marked as IV.

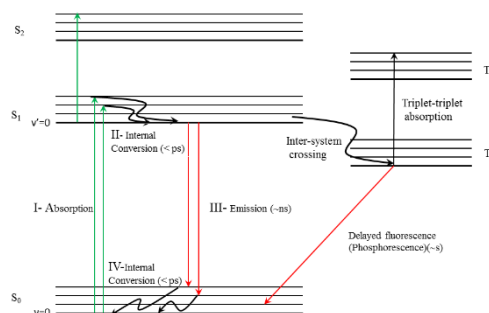


Fig. 3. Typical energy level diagram of dye molecule.

When the properties of the solvent changes such as refractive index ( $n$ ) and dielectric constants ( $\epsilon$ ), the ground and excited state of the dye to be stabilized instantaneously by movements of electron within the solvent molecules. This electron redistribution results a change in energy difference between the ground and excited states. The Stokes shift is related to the orientation polarizability term  $\Delta f$ , which is also known as solvent polarity function. The value of  $\Delta f$  can be measured by,

$$\Delta f = \left( \frac{\epsilon-1}{2\epsilon+1} - \frac{n^2-1}{2n^2+1} \right) \quad (1)$$

The difference in two terms (first term depends on the polarizability and second term depends on the RI) accounts for the spectral shifts due to re-orientation of the solvent molecules. Hence the energy state difference between the excited state and ground state of the dye is sensitive to the different properties of the solvents.

#### 4. Computational data

The geometry of Rhodamine B was optimized with Density Functional Theory (DFT) and the highest occupied molecular orbital (HOMO) and lowest unoccupied molecular orbital (LUMO) of the molecule in gas phase was calculated using B3LYP exchange correlation functional [8-9] and 6-31+G(d) basis set implemented in Gaussian 09 suite of codes [10]. The stationary points are characterized by frequency analysis. The solvent effects were included by Conductor-like Polarizable Continuum Model (CPCM) [11-12] solvation model. The vertical excitation energy and oscillator strength of Rhodamine B in different solvent are listed in table 1 and have been broadened with Gaussian function ( $\Delta\lambda=40$  nm). On comparing the TDDFT/ PCM calculated data with experimental results we demonstrate the accuracy of the TDDFT/ PCM approach for calculating vertical transition energy.

Table 1. Vertical excitation data of Rhodamine B in different solvent

Solvent	State	Main character	Wavelength (nm)	Oscillator strength (f)
Ethanol	State 1	H $\longrightarrow$ L	538.65	1.1666
	State 2	H-1 $\longrightarrow$ L	426.94	0.0466
	State 3	H-2 $\longrightarrow$ L	373.58	0.0165
Methanol	State 1	H $\longrightarrow$ L	539.84	1.1725
	State 2	H-1 $\longrightarrow$ L	427.24	0.0464
	State 3	H-2 $\longrightarrow$ L	369.54	0.0623
Butanol	State 1	H $\longrightarrow$ L	536.54	1.1558
	State 2	H-1 $\longrightarrow$ L	426.44	0.0469
	State 3	H-2 $\longrightarrow$ L	381.60	0.0048

However, the experimental and theoretically calculated energy gap shows a difference. This is because the calculation was done in gas phase while the absorption spectrum is taken in liquid phase. (More details are given in supporting information). The vertical excitation results using the computational method will give some accurate data of the photophysical properties in different environments.

## 5. Result and discussions

To study the emission characteristics from the dye dissolved in butanol, the emission spectra were recorded for various pump power. When the pump power was increased, the amplified spontaneous emission spectrum collapsed into multiple narrow lines as shown in figure 4. In the laser spectrum, each emission line had a linewidth less than 0.1 nm. Such a spectral narrowing cannot be found in ordinal ASE in which the linewidth gradually decreases to several nanometers [13]. A clear threshold behavior in the emission versus excitation intensities plot and a second decrease in the linewidth at higher excitation intensity indicated the onset of laser action (Right inset of figure 4). The strongly modulated laser spectrum with numerous evenly spaced peaks clearly indicates the resonant modes. Above the threshold, the total emission intensity increased much more rapidly with the excitation pump power. As the pump power increased, the lasing action occurred in the direction of the highest gain parallel to the excitation stripe. For increasing pump powers, the absorption decreases and the fluorescence grows due to the increased population inversion, thus the gain grows. Due to Stokes shift, the gain maximum grows and moves towards the higher energy side (smaller wavelengths). The gain maximum is very important since it has a big influence on the spectral position of the laser mode. Ideally, if all cavity modes have the same loss, the laser mode is the cavity mode which is positioned closest to the gain maximum. Similar blue-shift with the pump power has been also observed in various dye lasers systems [14-15].

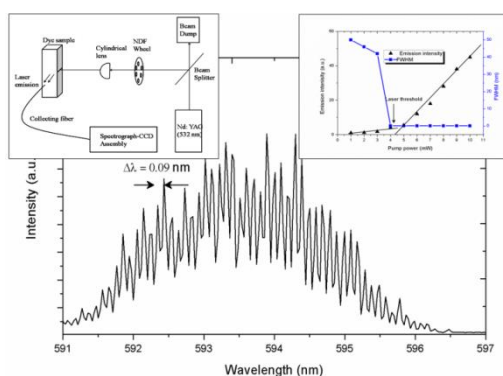


Fig. 4. Lasing spectrum of Rh B solution in Butanol at a pump power of 15 mW. Left inset shows the schematic of experimental setup and right inset shows the emission intensity and FWHM of emission band versus pump power.

The spectral peak intensity of the polymer ring laser is positioned at the maximum of optical gain which in turn corresponds to the photo-luminescent spectrum peak [15] around 590 nm. A large number of sharp lines can be seen within the fluorescent emission profile. The lasing modes are spectrally narrow with a FWHM of 0.05 nm with a pump power of  $P_{th} \times 4$  ( $\sim 15$  mW), where  $P_{th}$  is the lasing threshold pump power. When the pump power is higher than the lasing threshold ( $P_{th} \times 1.2$ ) lasing modes appear in the longer wavelength range (593–596 nm) of the photo-luminescence spectra of the gain medium. When the pump power is further increased, the lasing modes with high intensities start to develop on the shorter wavelength region of the spectra. The number of lasing modes and the resonant mode intensities increase with pump power as can be clearly seen in figure 5. The blue-shift as a function of pump power is attributable to the transfer of mode energy to that of the shorter wavelength side, which has gotten a large gain coefficient. However, the magnitude of this transition of energy gets saturated after a particular pump power.

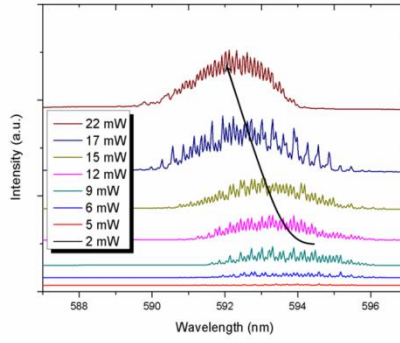


Fig. 5. The graph illustrates the lasing output intensities of Rh B dye ( $5 \times 10^{-4}$  mol/dm<sup>3</sup>) dissolved in butanol at different pump power. The spectrum moves towards shorter wavelengths with growing pump power.

The net gain of the dye doped laser system was generally measured by the variable stripe length (VSL) method. An adjustable slit was used to select the central portion and vary the width of the pump beam. The output intensity have been measured by,

$$I(\lambda) = \frac{\eta g'(\lambda)}{g(\lambda)} (e^{g(\lambda)l} - 1), \quad (2)$$

where  $g(\lambda) (=g'(\lambda)-\alpha)$ ,  $\alpha$  is the loss coefficient) is the net gain coefficient,  $g'(\lambda)$  is the internal gain coefficient due to stimulated emission process and  $l$  is the length of the pumped stripe. The value of the gain can be determined by plotting the emission intensity as a function of pumped stripe length and fitting the resulting curve to the expected dependence given by the equation 2. The systematic measurements of the intensity of the emitted light as a function of stripe length for three different pump power at 3 mW, 15 mW and 20 mW respectively have been shown in figure 6.

The black line in fig.6 is a fit of the data to equation 2, which yields a net gain of  $7.2 \text{ cm}^{-1}$  at a pump power of 3 mW ( $<P_{th}$ ). Above  $P_{th}$ , the measured gain is  $34 \text{ cm}^{-1}$  and  $42.1 \text{ cm}^{-1}$  by fitting the data using blue and red line for 15 and 20 mW respectively. In the equation 2, we are not considered the gain saturation and thus the net gain coefficient only those subsets of data for which gain saturation is not evident.

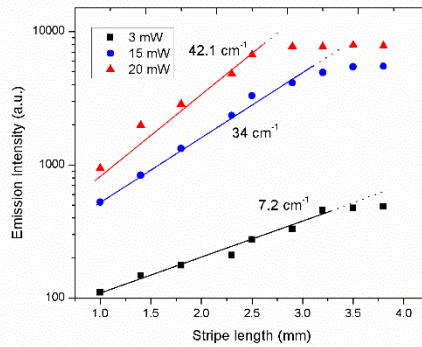


Fig. 6. Dependence of the emission intensity on stripe length at three different pump power for dye dissolved in butanol as 3, 15 and 20 mW respectively. The solid lines are fits to the data using equation 2.

One of another important optical quantity used to characterize a laser medium is stimulated emission cross-section ( $\sigma_e$ ). The value of  $\sigma_e$  can be derived from the emission spectrum  $E(\lambda)$  (which was not shown for the simplicity) by using [md11]

$$\sigma_e = \lambda^4 E(\lambda) / 8\pi c \tau m^4, \quad (3)$$

where  $c$  is the speed of light in free space,  $m$  is the refractive index of the medium (solvent),  $\tau$  is the fluorescent life time and it is assumed to be 2 ns. From the equation 3, we could obtained the value of  $\sigma_e \sim 8 \times 10^{-18} \text{ cm}^{-1}$ .

In our lasing experiment, external feedback at the cuvette sides might have encouraged the lasing action. It was expected that both the stimulated emission along with the gain guiding and the external feedback at the cuvette sides would induce a high gain for the laser action [16]. The occurrence of mode structure from dye solution was also reported by Guang *et al*, where the laser emission was attributed to the Fresnel reflection feedback from the two parallel optical windows of the cuvette [17]. Thus the partial reflectance from the window of the cuvette produces the effect of a Fabry-Perot etalon and provides the optical feedback necessary

for laser emission. In this case four subcavities are involved for cavity lasing; the cavity lasing wavelength should fulfil the following resonant conditions [18]:

$$\left. \begin{aligned} 2[nL + n'(l_1 + l_2)] &= K_1\lambda, \\ 2nL &= K_2\lambda, \\ 2(nL + n'l_2) &= K_3\lambda, \\ (nL + n'l_1) &= K_4\lambda, \end{aligned} \right\} \quad (4)$$

where  $L$  is the length of the medium,  $n'$  is the refractive index (RI) of quartz,  $l_1$  and  $l_2$  are the thickness of the cuvette,  $n$  is the RI of the gain medium and  $K_1, K_2, K_3$  and  $K_4$  are arbitrary integers [17]. The resonance condition providing the shortest spectral periodicity is obtained by the subtraction of the condition 1 and 3, which results

$$2n'l_1 = K\lambda, \quad (5)$$

where  $K = K_1 - K_3$ . The above equation is equivalent to the maximum transmission condition of the a Fabry-Perot etalon with an equivalent optical thickness of  $n'l_1$ . This implies that the cavity lasing spectrum will be modulated by this equivalent Fabry-Perot etalon provide the optical feedback necessary for laser emission. For the lasing spectrum the wavelength spacing between two adjacent modes is given by

$$\Delta\lambda = \lambda^2 / 2n'l_1, \quad (6)$$

where  $\lambda$  is the average lasing wavelength. Substituting for refractive index of quartz,  $n'$  as 1.46, the average lasing wavelength  $\lambda$  as 593 nm and the  $\Delta\lambda$  obtained from our studies with a cuvette of 1 cm path length as 0.09 nm. The thickness of the first parallel window is measured as  $\sim 1.1 \pm .03$  mm. The estimated value of  $l_1$  is found to be 1.15 mm at different position of the cuvette, which is in close agreement with the observed value.

The dye medium is found to be sensitive to the polarity and refractive index (RI) of the solvent in its nature of laser emission. The interaction between the solvents and the dye molecules affects the energy difference between the ground state and excited states. This energy difference is described by the Lippert equation. Most of the laser dyes are polar in nature and excitation into their low lying excited singlet state will be accompanied by an increase in the dipole moment. Hence the solvent polarity has a decisive role in shifting the laser wavelengths. In most of the cases, increasing the solvent polarity will shift the gain curve towards the longer wavelength side which is known as Stokes shift [19]. The emission spectra are recorded for different solvents such as Ethanol, Butanol, and Glycerol with fixed dye concentration of  $5 \times 10^{-4}$  mol/dm<sup>3</sup> as shown in figure 7. All the experimental conditions remained the same throughout the investigations with an ambient temperature of 21° C. The result shows a correlation between the physical characteristics such as RI, polarity of the different solvents and the multimode laser emission from the cavity. From the figure one could observe that the change in solvents introduces a corresponding shift in emission spectra. From ethanol to butanol the shift is approximately 4 nm, and from ethanol to glycerol the shift is approximately 6 nm. These types of shift in the emission spectrum with change in the solvent will allow a limited range of tuning of emission wavelengths. However, the spectral width and spacing between the adjacent lasing modes does not depends on the nature of the solvents but it is mainly depends on structure of the cavity.

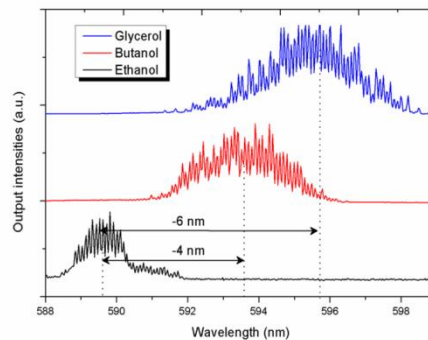


Fig. 7. Three measured laser spectra using Rh B dissolved ( $5 \times 10^{-4}$  mol/dm<sup>3</sup>) in ethanol, butanol and glycerol as the active gain medium, respectively with a pump power of 15 mW. The change of solvent introduces an over-all shift of the output spectra due to a shift of the gain-spectrum of the dissolved laser dye.

For a detailed analysis of the effect of solvent in the lasing characteristics of Rh B laser dye, the dye is also dissolved in different solvents such as methanol, toluene and ethylene glycol with the fixed dye concentration of  $5 \times 10^{-4}$  mol/dm<sup>3</sup>. Interesting results were obtained and these showed that the shift in emission spectrum is not only depends upon the value of RI and polarity of solvents but also the lower threshold population inversion [5] given by the solvents molecules. For the non-polar solvents like toluene, a deviation is observed from the polar and dipole aprotic solvents. This is due to the fact that toluene has a comparatively lower quantum yield and

high RI, which is almost higher than the quartz cuvette. Hence the reflection coefficient of the surface is also important for the lasing characteristics. Table 2 summarizes RI of the different solvents, polarity, peak wavelength, and number of lasing modes of Rh B dye dissolved in various solvents. From the table the laser emission is observed to be red-shifted in Ethylene Glycol solution which is less polar and RI as compared to Glycerol. This may be attributed to the more viscous nature of Glycerol, which may reduce the molecules interaction between dye and solvent molecules. The increased interaction between the dye molecules and the fluorescent light will result the shifting of emission wavelength toward the longer wavelength region. From this we can also conclude that the laser emission from the dye solution is not only depends on the RI and polarity of the solvent but also depends on the other nature of solvents such as viscosity and higher quantum efficiency or lower cavity loss of the solvents.

Table 2. Comparison of RI, polarity, emission peak, number of modes for different solvents [20-24].

Solvent name	RI	Polarity	Emission peak (nm)	Number of lasing modes	Dielectric constant ( $\epsilon$ )
Methanol	1.33	5.1	590	26	32.7
Ethanol	1.36	5.2	591	24	24.5
Butanol	1.39	3.9	594	42	--
Ethylene Glycol	1.43	5.4	598	46	37
Glycerol	1.47	5.8	596	62	42.5
Toluene	1.49	2.4	585	(Only ASE)	2.38

Fig. 7 shows a typical lasing spectrum from Rh B dissolved in methanol. The lasing peaks were considerably modulated as a clustered pattern. The resonance condition providing the widest spectral periodicity is obtained by the subtraction of the last two condition of Eqn. 3, which results,

$$2n'(l_2 - l_1) = K\lambda, \quad (7)$$

Where  $K = (K_3 - K_4)$ . From Eqn. 4 the modulation period can be determined by,

$$\delta\lambda = \lambda^2 / 2n'(l_2 - l_1), \quad (8)$$

From the equation we can observed that the modulation period is inversely proportional to the difference in the wall thickness ( $l_2 - l_1$ ) of the cuvette. The measured mode spacing  $\delta\lambda$  is  $\sim 1.2$  nm which is in good agreement with the calculated value of mode spacing ( $\sim 1.19$  nm), where ( $l_2 - l_1$ ) is estimated as 100  $\mu\text{m}$ .

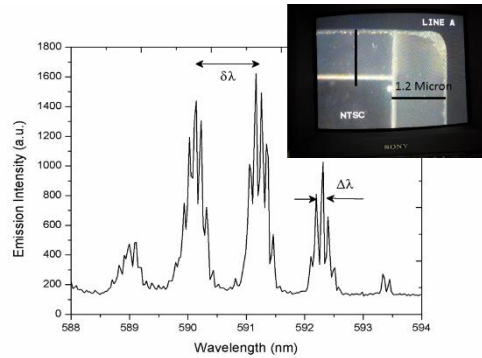


Fig. 8. Resonant modulation of laser modes of Rh B dye dissolved in methanol at a pump power of 15 mW. Inset shows the enlarged view of the variation in the thickness of the two walls of the cuvette.

The photograph of the CCD image taken for two walls of a cuvette is given in fig.8 inset, which clearly indicates the change in thickness of the different walls of the cuvette. The obtained laser emission spectra are modulated by the superposition of the laser modes due to optical thickness of  $n'l_1$  and difference in the wall thickness  $n'(l_2 - l_1)$  as shown in figure 8. We therefore attribute the appearance of emission spectra to a resonant modulation of the two type's laser resonant modes within the cavity.

## 6. Conclusion

Multimode laser emissions from Rh B laser dye in different solvents are investigated. The features of the mode structure in the emission spectra are employed to study the effects of solvents on the laser emission of the dye. The laser modes are found to originate from the subcavities formed by the plane parallel walls of the cuvette containing the gain medium. Changing solvent will allow a shift in the emission wavelength, which will allow a limited range of tuning of emission wavelength. The amount of shift in emission wavelength depends on the

different physical property of the solvents, such as polarity, refractive index, viscosity etc. The solvatochromic and Stokes-shift of Rh B in various solvents were successfully compared to experimental data with computational data. In our study we also determined the gain coefficient and stimulated emission cross-section of the Rh B dye laser system. The dye dissolved methanol solution will also provide a modulated laser emission due to two set of laser resonance achieved by the difference in the wall thickness of the cuvette.

### Acknowledgement

The authors acknowledge University Grant Commission (UGC) and Department of Science and Technology (DST) for the financial support. Jaison Peter is grateful to UGC for the research fellowship. The theoretical calculations have been performed in Gaussian suite of codes installed at Department of Applied Chemistry for which the authors gratefully acknowledge the support from Prof. K. Sreekumar.

### References

1. Frank L. Pedrotti and Leno S. Pedrotti. Introduction to Optics. Patience Hall International, Second edition, (1996).
2. F. P. Schafer (Editor). Dye Lasers. Springer-Verlag, (1973).
3. F. P. Schafer.; Dye lasers; topics in applied physics 1, 3<sup>rd</sup> Edn. Springer, Heidelberg.
4. M. Gersborg-Hansen, S. Balslev, N. A. Mortensen, A. Kristensen, Microelectronic Engineering 78-79, 185-189, (2005).
5. O. G. Pereson, J. P. Webb, and Mcclolgin W.C. J. Appl. Phys. 42 (5); 1917-1928, (1971).
6. G. D. Peng, Z. Xiong, P. L. Chu, Journal of Lightwave Technol. 16, 2365-2372, (1998).
7. A. Tagaya, Y. Koike, E. Nichei, S. Teramoto, K. Fujii, T. Yamamoto, K. Sasaki, Appl. Opt., 34, 988-992, (1995).
8. R. G. Parr and W. Yang, Density-functional theory of atoms and molecules (Oxford Univ. Press, Oxford, (1989)).
9. Becke, A. D. J. Chem. Phys. 98, 5648-5652, (1993).
10. Gaussian 09, Revision D.01, Frisch, M. J.; Trucks, G. W.; Schlegel, H. B.; Scuseria, G. E.; Robb, M. A.; Cheeseman, J. R.; Scalmani, G.; Barone, V.; Mennucci, B.; Petersson, G. A.; Nakatsuji, H.; Caricato, M.; Li, X.; Hratchian, H. P.; Izmaylov, A. F.; Bloino, J.; Zheng, G.; Sonnenberg, J. L.; Hada, M.; Ehara, M.; Toyota, K.; Fukuda, R.; Hasegawa, J.; Ishida, M.; Nakajima, T.; Honda, Y.; Kitao, O.; Nakai, H.; Vreven, T.; Montgomery, J. A., Jr.; Peralta, J. E.; Ogliaro, F.; Bearpark, M.; Heyd, J. J.; Brothers, E.; Kudin, K. N.; Staroverov, V. N.; Kobayashi, R.; Normand, J.; Raghavachari, K.; Rendell, A.; Burant, J. C.; Iyengar, S. S.; Tomasi, J.; Cossi, M.; Rega, N.; Millam, J. M.; Klene, M.; Knox, J. E.; Cross, J. B.; Bakken, V.; Adamo, C.; Jaramillo, J.; Gomperts, R.; Stratmann, R. E.; Yazyev, O.; Austin, A. J.; Cammi, R.; Pomelli, C.; Ochterski, J. W.; Martin, R. L.; Morokuma, K.; Zakrzewski, V. G.; Voth, G. A.; Salvador, P.; Dannenberg, J. J.; Dapprich, S.; Daniels, A. D.; Farkas, Ö.; Foresman, J. B.; Ortiz, J. V.; Cioslowski, J.; Fox, D. J. Gaussian, Inc., Wallingford CT, 2009.
11. Stephens, P. J.; Devlin, F. J.; Chabalowski, C. F.; Frisch, M. J. J. Phys. Chem., 98, 11623-11627, (1994).
12. V. Barone and M. Cossi, "Quantum calculation of molecular energies and energy gradients in solution by a conductor solvent model," J. Phys. Chem. A, 102 (1998) 1995-2001.
13. D. S. Weirisma, M. P. Van Albada, and A. Lagendijk, Nature (London) 373, 203, (1995).
14. Jaison Peter, Rasool Saleem, Ananthu Sebastian, P. Radhakrishnan, V. P. N. Nampoore, C. P. Girijavallabhan, M. Kailasnath, Optics Communications 320, 125-128 (2014).
15. Jaison Peter, C P G Vallabhan, P Radhakrishnan, V P N Nampoore and M Kailasnath, Laser Phys. 23 115104 (3pp), (2013).
16. Jaison Peter, P. Radhakrishnan, V. P. N. Nampoore, M. Kailasnath, Journal of Luminescence 149, 204-207 (2014).
17. Shiyoshi Yokoyama, Akira Otomo, and Shinro Mashiko, Appl. Phys. Lett., Vol. 80, No. 1, (2002).
18. Guang S. He, Raffaella Signorini, and Paras N. Prasad, Appl. Opt. Vol. 37, No. 24, 20 August (1998).
19. Ritty J. Nedumpara, Thomas K. J., Jayasree V. K., C. P. Girijavallabhan, V. P. N. Nampoore and P. Radhakrishnan, Appl. Opt. Vol. 46, No. 21, 20 July 2007.
20. J. R. Lakowicz, Principle of fluorescence spectroscopy plenum press, Newyork, 1983 (Chapter 9).
21. B. Bilenberg, B. Hebo, J. P. Kutter, A. Kristensen, Proc. Of the 12th Int. Conf. on solid-state sensors, Actuators and Microsystems, Transducers 03, Boston, MA-USA-2003. Pp. 206-209.
22. www.kabusa.com/Dielectric-constants.pdf
23. www.engineeringtoolbox.com/refractive-index-d-1264.html
24. Depts.washington.edu/eoopic/linkfiles/dielectric-chart%5B1%5D.pdf

### Supporting information from the computational data

#### Ethanol

Excited State 1: Singlet-A 2.3018 eV 538.65 nm f=1.1666 <S\*\*2>=0.000

127 ->128 0.70556

This state for optimization and/or second-order correction.

Total Energy, E(TD-HF/TD-KS) = -1881.06720673

Copying the excited state density for this state as the 1-particle RhoCI density.

Excited State 2: Singlet-A 2.9040 eV 426.94 nm f=0.0466 <S\*\*2>=0.000

122 ->128 -0.15299

126 ->128 0.67817

Excited State 3: Singlet-A 3.3188 eV 373.58 nm f=0.0165 <S\*\*2>=0.000

123 ->128 0.11108

125 ->128 0.69264

#### Methanol

Excited State 1: Singlet-A 2.2967 eV 539.84 nm f=1.1725 <S\*\*2>=0.000

127 ->128 0.70557

This state for optimization and/or second-order correction.

Total Energy, E(TD-HF/TD-KS) = -1881.06825969

Copying the excited state density for this state as the 1-particle RhoCI density.  
Excited State 2: Singlet-A 2.9020 eV 427.24 nm f=0.0464 <S\*\*2>=0.000  
122 ->128 -0.13151  
123 ->128 -0.12255  
126 ->128 0.67846  
Excited State 3: Singlet-A 3.3551 eV 369.54 nm f=0.0623 <S\*\*2>=0.000  
122 ->128 -0.10262  
123 ->128 -0.22352  
124 ->128 0.11430  
125 ->128 0.64617

#### Butanol

##### Excitation energies and oscillator strengths:

Excited State 1: Singlet-A 2.3108 eV 536.54 nm f=1.1558 <S\*\*2>=0.000  
127 ->128 0.70555

This state for optimization and/or second-order correction.

Total Energy, E(TD-HF/TD-KS) = -1881.06530285

Copying the excited state density for this state as the 1-particle RhoCI density.

Excited State 2: Singlet-A 2.9074 eV 426.44 nm f=0.0469 <S\*\*2>=0.000  
122 ->128 -0.16965  
126 ->128 0.67760  
Excited State 3: Singlet-A 3.2491 eV 381.60 nm f=0.0048 <S\*\*2>=0.000  
125 ->128 0.70233